

Scale Effects Investigation in Physical Modeling of Recirculating Shallow Flow Using Large Eddy Simulation Technique

R. A. Tartandyo¹, B. M. Ginting^{1†} and J. Zulfan²

¹ Department of Civil Engineering, Parahyangan Catholic University, Jl. Ciumbuleuit No. 94, Bandung, West Java 40141, Indonesia

² Water Research Laboratory, University of New South Wales, 110 King St, Sydney 2093, Australia

†Corresponding Author Email: bobbyminola.g@unpar.ac.id

ABSTRACT

In this study, the Large Eddy Simulation (LES) model in OpenFOAM was used to investigate the scale effects in the physical modeling of recirculating shallow flow at low Froude numbers. A laboratory test of turbulent flow through a submerged conical island with a Reynolds number of 6,210 was selected. The lab prototype was scaled with factors of 3 and 10 for both undistorted and distorted models. Our study employed the Froude similarity as the gravitational force is more dominant than the others (viscous, drag, and cohesion forces). Because the fluid (water) used for the prototype and model is the same, it is impossible to match the Reynolds, Weber, and Froude numbers simultaneously, resulting in the scale effects. For a scale of 1:1, the LES model could simulate the experimental data by appropriately capturing the vortices behind the conical island. For the undistorted models with scales of 3 and 10, the numerical model captured weaker magnitudes of vortices than the 1:1 scale, indicated by the discrepancies in velocity. In fact, the magnitudes of vortices became weaker with the distorted models. We also observed a significant increment in energy loss behind the conical island (where recirculating flows exist) as the scale increased. However, no significant discrepancies in velocity were observed between the results of the 1:1 scale and the scaled models in front of the conical island, where vortices were absent. These results indicate that the scale effects due to the Froude similarity are quite significant provided that recirculating turbulent flow occurs.

Article History

Received May 1, 2023

Revised August 31, 2023

Accepted September 16, 2023

Available online November 1, 2023

Keywords:

Large Eddy Simulation (LES)

OpenFOAM

Physical modeling

Recirculating flow

Scale effects

1. INTRODUCTION

Shallow or free-surface flow is a flow driven by gravity, where the fluid surface is exposed to the air (Chaudhry, 1993), such as in rivers, oceans, drainage systems, etc. Based on the Reynold numbers, shallow flow can be categorized into three conditions: laminar, transitional, and turbulent. Smooth, regular traveling particles and a lack of flow mixing in their paths generally characterize the laminar flow. Meanwhile, irregular flow paths, fluctuations, and mixing occur in relation to turbulent flow. For this regime, exogeneous perturbations that enter the boundary layer and are filtered eventually become unstable waves. Variables that govern the pathway to turbulence are the rising coherent flow structures, the critical or transitional Reynolds number, the skin friction, and the heat transfer to/from the wall (Rodi, 2017).

In hydraulics, flow characteristics are commonly investigated in two ways, either by the use of physical or numerical modeling. The former is a laboratory model that mimics the real-life prototype. In contrast, the latter utilizes a set of mathematical equations relying on computer capabilities to represent the physical system and to find approximate solutions to the underlying physical problems. Both approaches have their advantages and disadvantages. For instance, physical modeling is obviously more accurate than numerical modeling to represent a prototype; however, constructing it for a real-world scale requires high cost and an extended period of time. In some cases, this method even proves to be impossible.

Theoretically, prototypes in hydraulic physical modeling are replicated based on three similarity criteria: geometric, kinematic, and dynamic (Hughes, 1993; Martin & Pohl, 2000; Heller, 2007, 2011). The geometric similarity

NOMENCLATURE			
g	gravitational acceleration	τ^{SGS}	sub-grid scale stress tensor
L	hydraulic length	λ	scale
L_m	model hydraulic length	λ_r	scale ratio
L_p	prototype hydraulic length	ε	average rate of dissipation
p	pressure	μ	dynamic viscosity
t	time	k_{SGS}	sub-grid scale kinetic energy
ρ	density	ν	kinematic viscosity
\bar{U}	velocity	V	mesh volume
\bar{u}	velocity	ν_T	sub-grid scale eddy viscosity
v_m	model velocity	\bar{S}_{ij}	rate-of-strain tensor
v_p	prototype velocity		

comprises a similarity in shape, signifying that the dimension of the prototype must be scaled with a factor (λ); hence, the model will have a dimension that is λ times smaller. The kinematic similarity involves establishing a ratio between a model and its prototype in terms of their motion properties, such as velocity, time, acceleration, and discharge, in addition to the geometric similarity. The dynamic similarity dictates that the force ratio in the system of both model and prototype must be identical, including the kinematic and geometric similarities.

Furthermore, two scaling types are commonly applied to physical modeling, namely undistorted and distorted models. The former is meant to have geometric dimensions proportionate to the scaled prototype. Conversely, the latter has a different geometric scaling ratio indicating that both the horizontal and vertical scales differ.

One challenge primarily encountered in physical modeling pertains to scale effects, which are defined as discrepancies in modeled-flow characteristics in relation to their prototype attributes. These differences were caused by the incapability of the scale to represent all the relevant force ratios (Chanson et al., 2004; Novak et al., 2007; Heller, 2007; Chanson, 2008; Chanson & Murzyn, 2008; Chanson, 2009; Heller, 2011; Tullis 2018; Torres et al., 2022). If the scale between the model and the prototype is not identical, then only one force ratio can be equivalent between the two systems. Thus, dynamic similarity is impossible to achieve, and to deal with this issue, only the most prominent force ratio in both systems is selected (Heller, 2007; Novak et al., 2010; Heller, 2011).

To our knowledge, only small attention is given to the scale effects' investigation for recirculating turbulent flows. Torres et al. (2022) confirmed that the most significant discrepancies between the model and prototype scales occurred in the lowest flows due to the relative influence of viscosity and surface tension. Nonetheless, the differences in the flow behaviors between both scales reduced for increasing flow rate. While their work focused on the scale effects for the cross-wave patterns by observing the mean depth and average velocity, no attention was paid to the scale effects for recirculating flow (vortices).

Suerich-Gulick et al. (2014) proposed a correction factor to estimate the magnitude of surface tension effects in a laboratory-scale vortex. Nevertheless, it failed to

reproduce the independence from the Reynolds number at large Reynolds values up to a certain level, implying that additional processes must intervene or that the flow structure may change at larger scales. Suerich-Gulick et al. (2014) underlined that the scale effects associated with viscosity and turbulence are much more difficult to predict. Consequently, potential changes in the flow structure at larger scales, perturbations, and enhanced diffusion caused by turbulence must be examined more thoroughly to better understand the observed scaling behavior. This indicates that understanding the scale effects for recirculating turbulent flow remains challenging.

The objective of our study is to examine the impact of various turbulent structures on flow properties with the Froude similarity scaling (both distorted and undistorted), particularly for recirculating turbulent shallow flows at low Froude numbers. Hypothetically, the scale effects become highly significant when vortices or recirculating flows appear. Generally, the recirculating zone is dominated by energetic flow structures and significant flow separation, posing difficulty in numerical modeling (Ouro et al., 2017). Seeking to prove this hypothesis, we conducted a numerical simulation with the Large Eddy Simulation (LES) model for the laboratory experiment done by Lloyd and Stansby (1997) that dealt with recirculating turbulent shallow flows.

Principally, the LES model lies between the Direct Numerical Simulation (DNS) and Reynolds-Averaged Navier Stokes (RANS) models; hence, it gives the best of both methods in terms of accuracy and computational time (Rodi, 2017). The LES model includes a low-pass spatial filter, thus resolving larger vortices or eddies than the RANS model and requiring coarser computational grids than the DNS model (Ferziger & Perić, 1996; Lesieur & Metais, 1996; Piomelli, 1999; Fröhlich & Rodi 2002; Stoesser, 2014; Rodi, 2017). The LES technique requires the sub-grid scale (SGS) model as there are motions at all scales (from the large scale to the Kolmogorov one) (Fröhlich & Rodi 2002). To accomplish the research objective, the investigation will be carried out as follows:

1. Validating the results of the numerical model with the observed data from Lloyd and Stansby (1997) for the prototype scale
2. Examining the scale effects for both undistorted and distorted models.

Note that our study is limited to investigating the scale effects for recirculating turbulent shallow flows under the Froude similarity as the gravitational force is more dominant than the others (viscous, drag, and cohesion forces). In this way, it is impossible to match the Reynolds, Weber, and Froude numbers simultaneously because the fluid (water) used for the prototype and model is the same, thus resulting in the scale effects. We will show in this paper that when recirculating turbulent flows occur, the scale effects owing to the Froude similarity are considerable, where the differences in velocity magnitude and vortices' period are detected. This points out that the Froude similarity does not adequately account for the influence of changes in turbulent structure of the flow.

Our research contributes to a better understanding of the complex interplay between turbulent structures, Froude similarity scaling, and flow characteristics by highlighting the considerable scale effects induced by recirculating turbulent shallow flows. In this regard, the velocity is used to compare the scale effects between the prototype and model scales, while the flow depth is relatively constant over the domain.

2. METHODS

2.1 Governing Equations

The Navier-Stokes equations for incompressible, Newtonian fluids are generally expressed as

$$\text{div}(\bar{U}) = 0 \quad (1)$$

$$\rho \left(\frac{d\bar{U}}{dt} + (\text{div}(\bar{U})\bar{U}) \right) = -\text{div}(p) + \mu(\text{div}(\text{grad } \bar{U})) + \rho g \quad (2)$$

where \bar{U} defines the velocities in all directions, ρ is the fluid density, p is the pressure, μ is the dynamic viscosity, and g is the gravitational acceleration.

On the left side of the Eq. (2), $\rho \frac{d\bar{U}}{dt}$ denotes the local acceleration, and $\rho(\text{div}(\bar{U})\bar{U})$ denotes the convective acceleration. While on the right side of Eq. (2), $-\text{div}(p)$ is the pressure gradient of the fluid, which flows in the direction of the largest change in pressure. $\mu(\text{div}(\text{grad } \bar{U}))$ indicates the viscous effects, where the viscosity operates as a diffusion of momentum for the Newtonian fluid, and ρg denotes the external forces, e.g., gravity, see [Versteeg and Malalasekara \(2007\)](#).

The idea behind the LES model is to include a low-pass spatial filter, which allows for resolving the bigger vortices or eddies in the turbulent domain while only modeling the smaller vortices or eddies. This approach enables the computing grids to be coarser than the ones required in the DNS model. Physically, there is an interaction in the movements at all scales (from large to Kolmogorov), necessitating the incorporation of a so-called sub-grid scale (SGS) model, see [Fröhlich & Rodi \(2002\)](#). Resolving vast scales of the flow while just modeling the miniscule ones will be advantageous, resulting in findings with far greater accuracy than the Reynolds-averaged Navier-Stokes (RANS) model. The

LES SGS models were also recently employed in several previous works, see [Sharma et al. \(2021\)](#) and [Singh et al. \(2022\)](#).

The SGS technique is employed in the LES model, thus leading to

$$\nabla \cdot (\bar{u}) = 0 \quad (3)$$

$$\rho \left(\frac{d\bar{u}}{dt} + \nabla(\bar{u}\bar{u}) \right) = -\nabla P + \mu \nabla^2 \bar{u} + \rho g + \nabla \cdot \tau^{SGS} \quad (4)$$

where \bar{u} denotes the velocities in all directions and the sub-grid scale stress tensor τ^{SGS} is an apparent stress that arises from the filtering operation, being equivalent to

$$\tau^{SGS} = -(\overline{uu} - \bar{u}\bar{u}) \quad (5)$$

In the LES model, the incompressible Navier-Stokes equations are spatially filtered to a characteristic width $\bar{\Delta}$. The details are not discussed here. Hence, interested readers are referred to [Pope \(2000\)](#), [Sagaut \(2006\)](#), [Fröhlich & Rodi \(2002\)](#), and [Rodi \(2017\)](#).

A dynamic one-equation model for the SGS kinetic energy $k_{SGS} = \frac{1}{2}(\bar{u}_i^2 - \bar{u}_i'^2)$, in the upcoming form can be written as ([Yoshizawa, 1993](#)):

$$\frac{\partial k_{SGS}}{\partial t} + \bar{u}_i \frac{\partial k_{SGS}}{\partial x_i} = -\tau_{ij} \frac{\partial \bar{u}_i}{\partial x_j} - \varepsilon + \frac{\partial}{\partial x_i} (\nu_T \frac{\partial k_{SGS}}{\partial x_i}) \quad (6)$$

which has also been studied in [Menon and Yeung \(1994\)](#) and [Menon et al. \(1994\)](#). On the right side of Eq. (6), the terms denote, respectively, the production rate, the dissipation rate, and the transport rate of the k_{SGS} . The subgrid stress τ_{ij} is modeled in terms of the SGS eddy viscosity ν_T , which is:

$$\tau_{ij} = \frac{2}{3} k_{SGS} \delta_{ij} - 2\nu_T \bar{S}_{ij} \quad (7)$$

where the SGS eddy viscosity ν_T is computed using k_{SGS} as

$$\nu_T = C_v \sqrt{k_{SGS}} \bar{\Delta} \quad (8)$$

where the filter size $\bar{\Delta}$ is computed from

$$\bar{\Delta} = V^{1/3} \quad (9)$$

and the dissipation rate ε can be modeled as

$$\varepsilon = C_\varepsilon \frac{k_{SGS}^{3/2}}{\bar{\Delta}} \quad (10)$$

A vital characteristic of this model is that no assumption of the local equilibrium has been made between the SGS energy production and the dissipation rate. Hence, the direct computation of the SGS kinetic energy is employed for this model, which can be used to capture some non-local and historical effects in the smallest scale. The C_ε and C_v coefficients are derived from the local flow properties ([Kim & Menon, 1995](#)).

2.2 Froude Similarity

As previously explained, the dynamic similarity states

that all the force ratios between the prototype and the model must remain the same. Nevertheless, it is impossible to achieve, especially if the fluid used for the prototype and model is the same. The Froude similarity is more frequently used for shallow flow as the gravitational force is more dominant than the others (viscous, drag, and cohesion forces). The Froude similarity is appropriate for models with negligible friction effects and turbulent regimes. This is in accordance with the case study investigated in this paper, see Sub-section 2.3.

The Froude similarity indicates that the Froude number (Fr) of the model and the prototype is the same, which can be expressed mathematically as:

$$L_m = \lambda \times L_p \tag{11}$$

$$Fr_{\text{model}} = Fr_{\text{prototype}}$$

$$\frac{V_m}{(gL_m)^{\frac{1}{2}}} = \frac{V_p}{(gL_p)^{\frac{1}{2}}} \tag{12}$$

$$\frac{V_m}{(g\lambda L_p)^{\frac{1}{2}}} = \frac{V_p}{(gL_p)^{\frac{1}{2}}} \tag{13}$$

where λ is the scale of length/depth, V is the velocity, L is the length/depth, g is the gravitational acceleration, and the subscripts m and p denote the model and prototype, respectively. Because the gravitational acceleration is the same, it can be neglected, thus yielding:

$$V_m = V_p \sqrt{\lambda} \tag{14}$$

Note that the above equation applies to the undistorted scale. For the distorted model, the scale is defined by a ratio between the horizontal and vertical scales (λ_r), which can be written as:

$$\lambda_r = \frac{y_r}{x_r} \tag{15}$$

where x_r is the horizontal scale and y_r is the vertical scale. Applying the Froude similarity to the distorted model yields the velocity as:

$$V_m = V_p \sqrt{\lambda_r \lambda} \tag{16}$$

The equations above show that the Froude number is kept constant between the prototype and model (both distorted and undistorted) by adjusting the free-stream velocity value.

2.3 Model Description

This research adopted a laboratory case from [Lloyd and Stansby \(1997\)](#). The sketch of the case is shown in Fig. 1. This case dealt with shallow water flows in a turbulent regime around a submerged conical island, where the free-stream velocity was 0.115 m/s with a water depth of 0.054 m, thus giving the Froude number of 0.158 and the Reynolds number of 6,210. [Lloyd and Stansby \(1997\)](#) constructed the laboratory flume using a combination of marine quality plywood and polyvinyl chloride (PVC) materials to ensure the smoothness of the flume surface. Hence, it is reasonable to assume that the bed friction does not play a significant role, and thus, the Froude similarity can be applied to our study. [Ginting and Ginting \(2019\)](#) also discovered that changing the Manning (roughness) coefficient for this case did not result in significant differences.

In Fig. 2, we present a sketch where the recirculation zone is expected to exist behind the conical island, the vortices emerging in such a zone. Recirculation occurs in this region because of the interplay between the entering

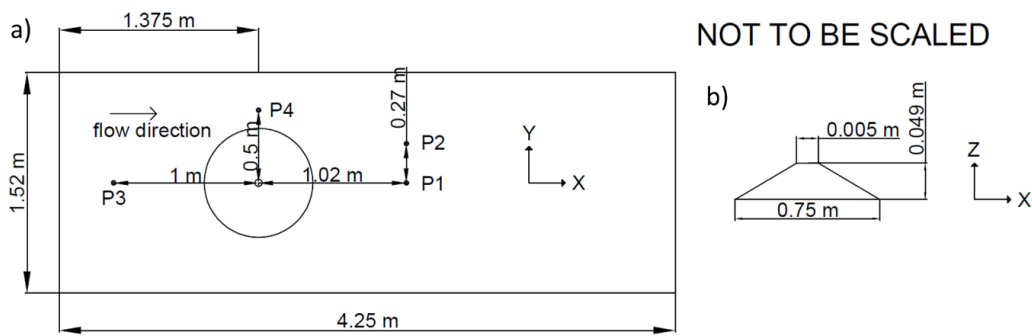


Fig. 1 Sketch of the experimental study based on [Lloyd and Stansby \(1997\)](#): (a) top view and (b) conical island section

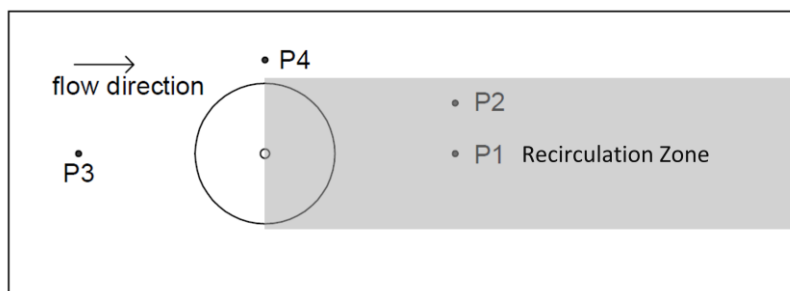


Fig. 2 Sketch of the recirculation zone

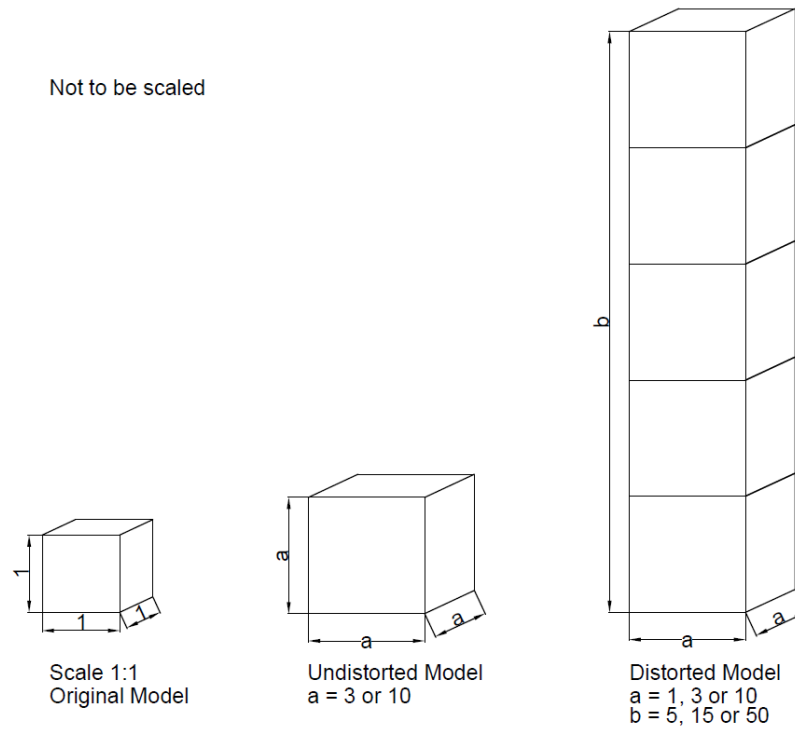


Fig. 3 Overview of the model setup for original, undistorted model, distorted model

flow and the blockage by the conical island. The existence of vortices and eddies in the recirculation zone contributes to the complex flow patterns. On the other hand, the non-recirculation zone refers to the areas in front of and next to the conical island, where the streamline is relatively straight without substantial disruptions or vortices.

Our simulations include six cases. The first one is used to numerically simulate the experimental study, where the computed velocity is compared with the benchmark data to investigate the accuracy of the numerical model. Furthermore, the second and third cases are used to investigate the scale effects of the undistorted model. Ergo, they are upscaled by the factors of 3 and 10, respectively.

The fourth, fifth, and sixth cases are employed to investigate the scale effects of the distorted model. The horizontal scale for the distorted case is the same as the previous three cases (1, 3, and 10, respectively). The ratio between the vertical and horizontal scales, however, is shifted. The vertical scale is five times larger than the horizontal one. For example, in case 4 (case 1:1 D), the horizontal scale is the same as in case 1 but the vertical scale is multiplied by a factor of 5, which indicates that the vertical dimension is five times greater than the horizontal one. The overview of the horizontal and vertical scales is shown in Fig. 3.

Two observation points (see P1 and P2 in Fig. 1) are located, identical to the work of [Lloyd and Stansby \(1997\)](#). For the first case, the position of P1 is (1.02, 0, 0.054) m, and P2 is (1.02, 0.27, 0.054) m, if the center of the conical island is (0, 0, 0) m. In addition to comparing the numerical results at P1 and P2, our study also includes the velocity output for the non-recirculating zone, which is

used to prove whether the scale effects are dominant for such a zone. Consequently, two other probes are added. For the first case, the location of P3 is set to (-1, 0, 0.054) m, and P4 is (0, 0.5, 0.054) m. Note that the original probes' position needs to be scaled accordingly to examine the scale effects for the remaining cases.

The geometry of the model was produced using ANSYS DesignModeller. The numerical simulation was accomplished using *pimpleFoam*, a transient solver for incompressible, turbulent flow of the Newtonian fluid, utilizing the PIMPLE (merged PISO-SIMPLE) algorithm. In order to expedite the simulation, parallelization was employed using the computing resource at our Water Resources Engineering Laboratory that is supported by Intel Core i9-10900K for 10 physical CPU cores. Also, we were able to use the computing resource at the BINTEK Laboratory, which is supported by Intel Xeon W-1290P for 10 physical CPU cores. Therefore, the mesh can be decomposed into 10 subdirectories.

In order to ensure the convergence of the numerical results, the simulations were performed in two phases. The first phase was run for 250 s with a Courant–Friedrichs–Lewy (CFL) number of 0.6, aiming to stabilize the flow properties. After the flow characteristics became relatively stable, the second phase was run for 100 s with a CFL number of 0.3. This phase was specifically used to extract the velocity output.

Note that we initially used a CFL number of 0.3, which was chosen according to the experience of our corresponding author in [Ginting & Ginting \(2019\)](#) for the same benchmark case. However, as it took a relatively-long period of time for our current work with the LES model (due to the limitation of our computing resources),

we decided to make another approach by doubling the CFL number to 0.6 in order to reduce the simulation time; during the first 250 seconds, a CFL number of 0.6 was used, and the rest was with 0.3. We compared the results of both approaches and found only insignificant differences. For this reason, choosing both CFL numbers in our study is a trade-off between time efficiency and computational stability.

It is also necessary to highlight that the experimental work of [Llyod & Stansby \(1997\)](#) did not focus on the free-surface. There was no measurement for the water surface fluctuations because such fluctuations (millimeter order) were very small compared to the still water depth that varied between 0.050 – 0.136 m, and thus, the free-surface effect was negligible. Our corresponding author had also proven this by simulating the same case using the RANS model, see Fig. 14 in [Ginting & Ginting \(2019\)](#), which showed the water elevation range to be 0.0535 – 0.0547 m. With regard to the reference water depth of 0.054 m, the free-surface fluctuations were 0.0005 – 0.0007 m. In contrast, the velocity differed significantly for such water surface levels ranging from 0.000001 – 0.25 m/s. This clearly indicates that the influence of velocity in this case is more significant than the water depth, for which it is reasonable to state that the water depth tends to be

constant. The model setup for all simulations is summarized in Table 1.

2.3 Numerical Setup

This section briefly explains the parameter setup for our numerical model. For the inlet boundary, the velocity was specified, and the zero-pressure gradient was set. For the outlet boundary, no velocity gradient was applied, and the pressure was specified. The no-slip condition was employed for the wall boundary. For the initial condition, the pressure and velocity were set constant.

We applied homogeneous meshes to all simulations as we desired to follow the computational mesh size used in the original work of [Llyod & Stansby \(1997\)](#), namely 0.0152 m. This was also followed by [Ginting & Ginting \(2019\)](#) and others, see the references therein. As sketched in Fig. 3, both undistorted and distorted models employed the same mesh sizes. For example, for the scale of 1:3 (distorted model), the mesh size in the vertical direction is kept the same as the scale of 1:3 (undistorted model). We did this to avoid the influence of the “mesh size effect” on the results between the undistorted and distorted models (theoretically, the finer the mesh size, the more accurate the result). Obviously, we had performed small experiments to observe the grid sensitivity using the following mesh sizes: 0.025, 0.02, 0.0152, and 0.01 m. We

Table 1 Summary of the model parameters

Case	Scale	Dimension				Water Depth	Velocity	Mesh Size	Mesh Count	Froude Number (<i>Fr</i>)	Reynolds Number (<i>Re</i>)
		Domain		Conical Island							
		m		m		m	m/s	m			
1	1:1	W:	1.52	Bot D:	0.75	0.054	0.115	0.0152	712,604	0.158	6,210
		L:	4.25	Top D:	0.005						
				H:	0.049						
Undistorted model (Scale ratio of 1)											
2	1:3	W:	4.56	Bot D:	2.25	0.162	0.199	0.0456	712,134	0.158	32,238
		L:	12.8	Top D:	0.015						
				H:	0.147						
3	1:10	W:	15.2	Bot D:	7.5	0.54	0.364	0.152	713,308	0.158	196,560
		L:	42.5	Top D:	0.05						
				H:	0.49						
Distorted model (Scale ratio of 5)											
4	1:1	W:	1.52	Bot D:	0.75	0.27	0.257	0.0152	4,154,599	0.158	69,390
		L:	4.25	Top D:	0.005						
				H:	0.245						
5	1:3	W:	4.56	Bot D:	2.25	0.81	0.445	0.0456	4,154,398	0.158	360,450
		L:	12.8	Top D:	0.015						
				H:	0.735						
6	1:10	W:	15.2	Bot D:	7.5	2.7	0.813	0.152	4,152,980	0.158	2,195,100
		L:	42.5	Top D:	0.05						
				H:	2.45						

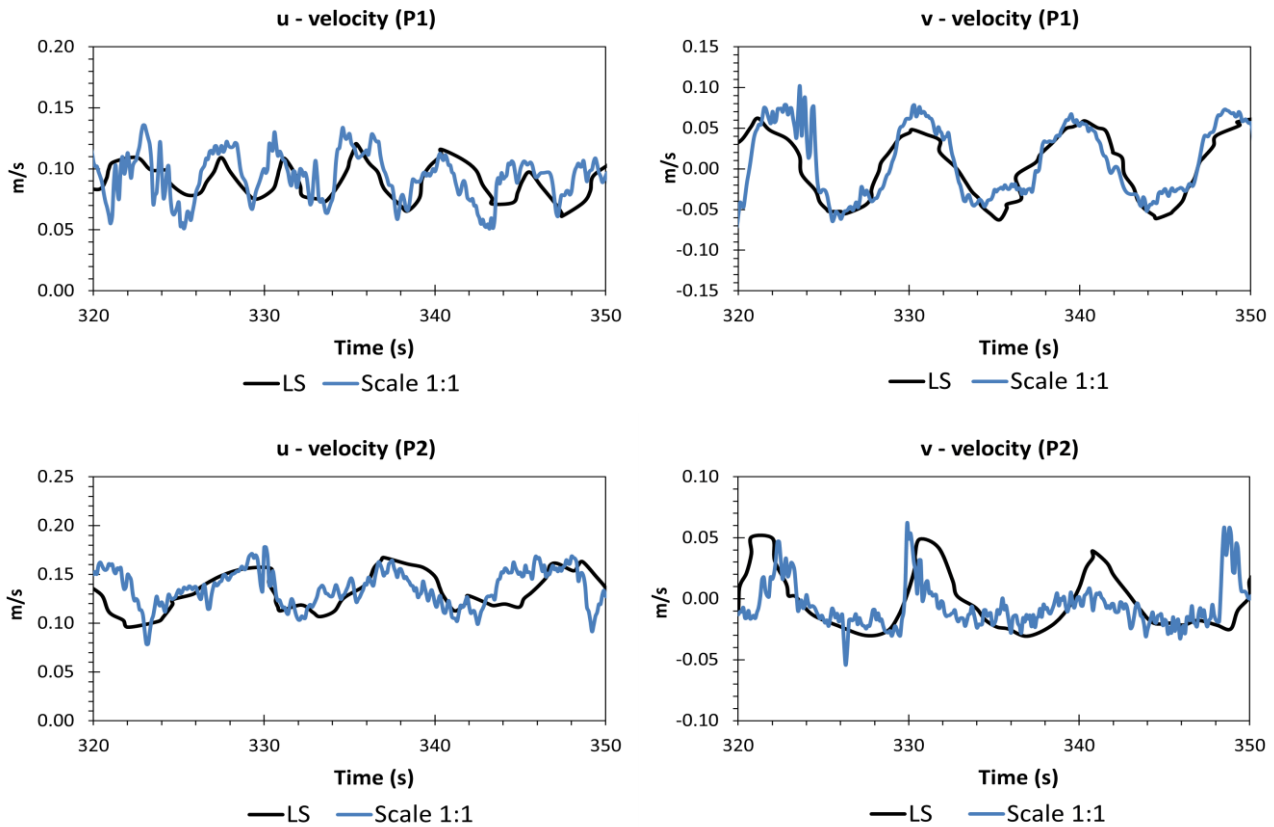


Fig. 4 Velocity profile – case 1

found that using a finer mesh size could capture stronger vortices. Notwithstanding, no significant differences were noted between the results with the mesh size of 0.0152 m and 0.01 m. For the sake of brevity, the results are not presented here.

The numerical model in OpenFOAM employs the Gaussian integration from cell centers to face centers for the spatial discretization. The PIMPLE algorithm is utilized for the pressure-velocity coupling. This transient solver operates in two loops: the first loop couples the pressure and velocity, whereas the second loop focuses on pressure and velocity correction. For the temporal discretization, the second-order accurate backward difference scheme is used for all simulations.

3. RESULTS AND DISCUSSION

The Froude number of 0.158 was maintained constant for each case, while the dimension, depth, velocity, and mesh size may vary. To maintain brevity, the experimental data are denoted as LS in the plots. The outcomes of the simulations are presented as two velocity values (i.e., u-velocity and v-velocity for the velocities in the x and y directions, respectively) at four probe points (P1, P2, P3, and P4).

3.1 Validating Numerical Model with Experimental Data

Prior to assessing the scale effects, one must verify whether the LES model with the dynamic k-equation can simulate the benchmark case accurately by comparing the model result with the observed data. In this regard, we

compared the velocity magnitude and vortices wake period with the experimental data. Additionally, two statistical methods, Root Mean Square Error (RMSE) and Pearson Product Moment Correlation (PPMC), were employed to measure the error and correlation between the simulation results and observed data. The PPMC values are classified into four groups of correlation: (a) greater than ± 0.5 for strong positive/negative, (b) between ± 0.3 and ± 0.5 for moderate positive/negative, (c) between 0 and ± 0.3 for weak positive/negative, and (d) 0 for no correlation.

Like [Ginting and Ginting \(2019\)](#), the simulation was conducted with a mesh size of 0.0152 m for a duration of 350 s to ensure numerical stability. The results obtained during the last 30 s were compared with the LS experiment after adjusting the difference in the phases of the turbulent wakes. The results in Fig. 4 indicate that the LES model properly captured the velocity fluctuation at P1 and P2. Despite oscillations, the pattern and magnitude values produced at these points are quite similar to the LS experiment indicating proper numerical results. Note that the observed values of the LS experiment were obtained from the depth-integrated velocity values, thus being quite smooth. Meanwhile, the simulated values in Fig. 4 were taken as 3D results at the water surface.

The summary of the RMSE and PPMC values for each case is given in Table 2. The PPMC values for case 1 indicate that the numerical model shows a positive correlation for all velocities at P1 and P2. A strong positive correlation is shown for v-velocity at P1, and a moderate positive correlation is shown for u-velocity at P1 as well

Table 2 Comparison of error values

Case	Scale	Probe	Velocity		RMSE	PPMC
1	1:1	P1	u	:	0.0172 m/s	0.5553
			v	:	0.0235 m/s	0.8292
		P2	u	:	0.0189 m/s	0.4496
			v	:	0.0277 m/s	0.3172
Undistorted Model (Scale ratio of 1)						
2	1:3	P1	u	:	0.0267 m/s	0.1690
			v	:	0.0246 m/s	0.0119
		P2	u	:	0.0397 m/s	-0.0613
			v	:	0.0360 m/s	-0.2650
3	1:10	P1	u	:	0.0282 m/s	-0.0155
			v	:	0.0258 m/s	-0.2136
		P2	u	:	0.0397 m/s	-0.2541
			v	:	0.0293 m/s	-0.1421
Distorted Model (Scale ratio of 5)						
4	1:1	P1	u	:	0.0450 m/s	0.1509
			v	:	0.0481 m/s	-0.0047
		P2	u	:	0.0454 m/s	-0.0613
			v	:	0.0392 m/s	-0.0245
5	1:3	P1	u	:	0.0377 m/s	-0.0398
			v	:	0.0440 m/s	0.2876
		P2	u	:	0.0388 m/s	0.2248
			v	:	0.0360 m/s	0.1395
6	1:10	P1	u	:	0.0293 m/s	0.3577
			v	:	0.0551 m/s	-0.1336
		P2	u	:	0.0446 m/s	0.2020
			v	:	0.1109 m/s	0.1604

as both u-velocity and v-velocity at P2. From this finding, it is reasonable to state that the LES model can simulate the LS experiment appropriately for the prototype scale (1:1). Thus, it can be used as a proper model for the other simulations (case 2 – case 6) in order to investigate the scale effects.

3.2 Scale Effects for Recirculating Flow Zone

In this section, the remaining cases with the upscaled ratios are investigated. As shown in Table 1, the undistorted models (case 2 and case 3) are scaled by the factors of 3 and 10, and the mesh size is proportionally scaled. For the distorted models (case 4, case 5, and case 6), the horizontal scales are 1, 3, and 10, while with a scale ratio of 5, the vertical scales are 5, 15, and 50, respectively. The mesh size is also proportionally scaled to its horizontal scale. The simulation results were assessed using the same statistical parameters as case 1 (RMSE and PPMC).

The mesh size used is proportionally scaled by the factors of 3 and 10 for case 2 and case 3, thus being 0.0456 m and 0.152 m, respectively. Meanwhile, for the distorted

models, the mesh size is 0.0152 m, 0.0456 m, and 0.152 m for case 4, case 5, and case 6, respectively. Like case 1, the remaining cases were simulated for 350 s, where the results obtained in the last 30 s were compared with the LS experiment after adjusting the different phases of turbulent wakes. The results are shown in Fig. 5 and Fig. 6, showing that the LES model could still capture the recirculation behind the conical island. Nonetheless, the velocity magnitude and wake period showed significant phase differences indicating the presence of the scale effects. One can see that the simulations for case 2 and case 3 tend to underestimate the results, especially at P2. In contrast with the undistorted model, the simulations for the distorted model tend to overestimate the results. This can be seen from the pattern in Fig. 6, where the maximum and minimum values significantly differ from the LS experiment.

For case 2 and case 3, the RMSE values are relatively higher than the ones for case 1. For case 2, both PPMC values at P1 exhibit a weak positive correlation with the LS experiment data. Meanwhile, the PPMC values at P2 show a weak negative correlation. For case 3, all the

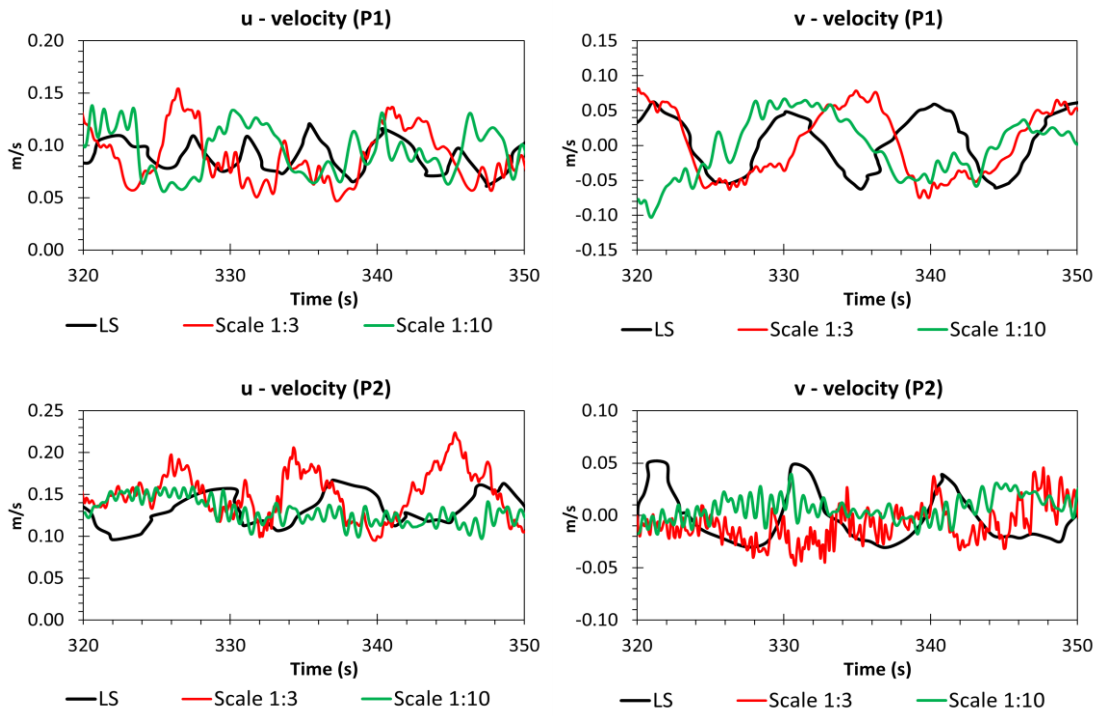


Fig. 5 Velocity profile – case 2 and case 3

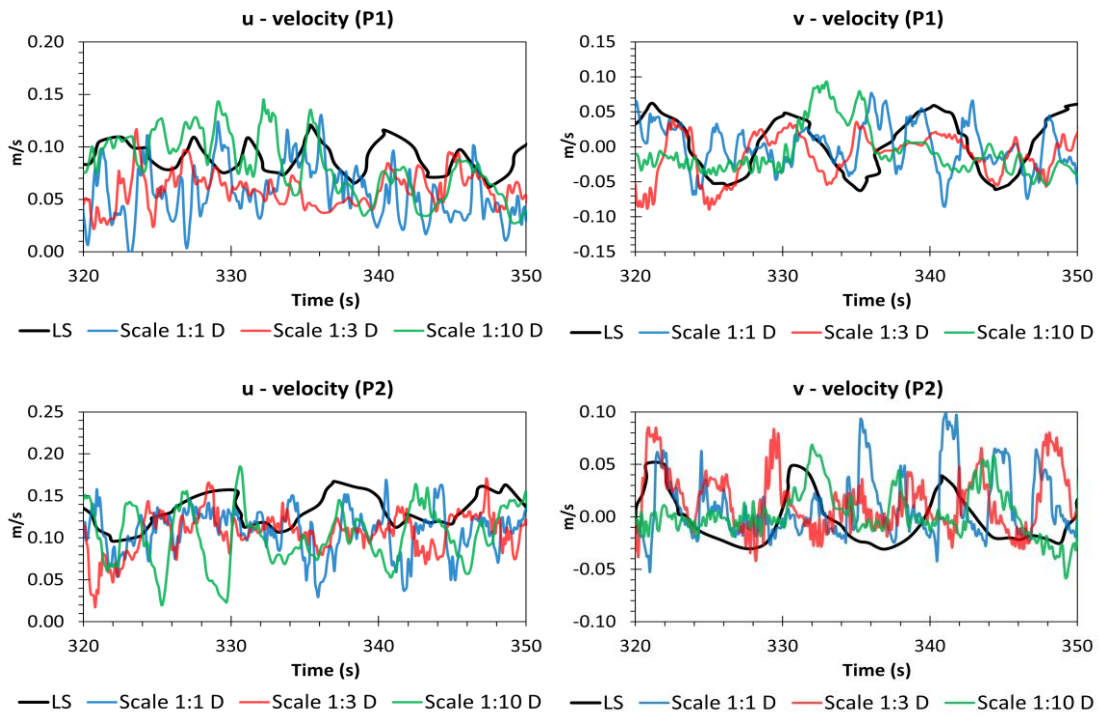


Fig. 6 Velocity profile – case 4, case 5, and case 6 (D denotes the distorted model)

PPMC values indicate a weak negative correlation, meaning that the higher the numerical results, the lower the values of the observed data, which obviously exhibit opposite behavior with the LS experiment data.

The results of cases 4, 5, and 6 show that the distorted model produces higher RMSE values than the undistorted models. Interestingly, the PPMC values of the undistorted models are not necessarily better than the distorted ones. This can be clearly noted from case 3 and case 5. The RMSE value of case 3 for the v -velocity at P1 is 0.0258

m/s, almost twice as low as that of case 5; however, the PPMC value for case 5 (0.2876) is significantly better than case 3 (-0.2136). Albeit weak, case 5 still shows a positive correlation between the numerical results and the observed data.

No obvious evidence from cases 2–6 suggests a linear relationship between the scale size and the error induced by both undistorted and distorted models. Nevertheless, the existence of the scale effects for the recirculation zone can be observed by the RMSE and PPMC values. For

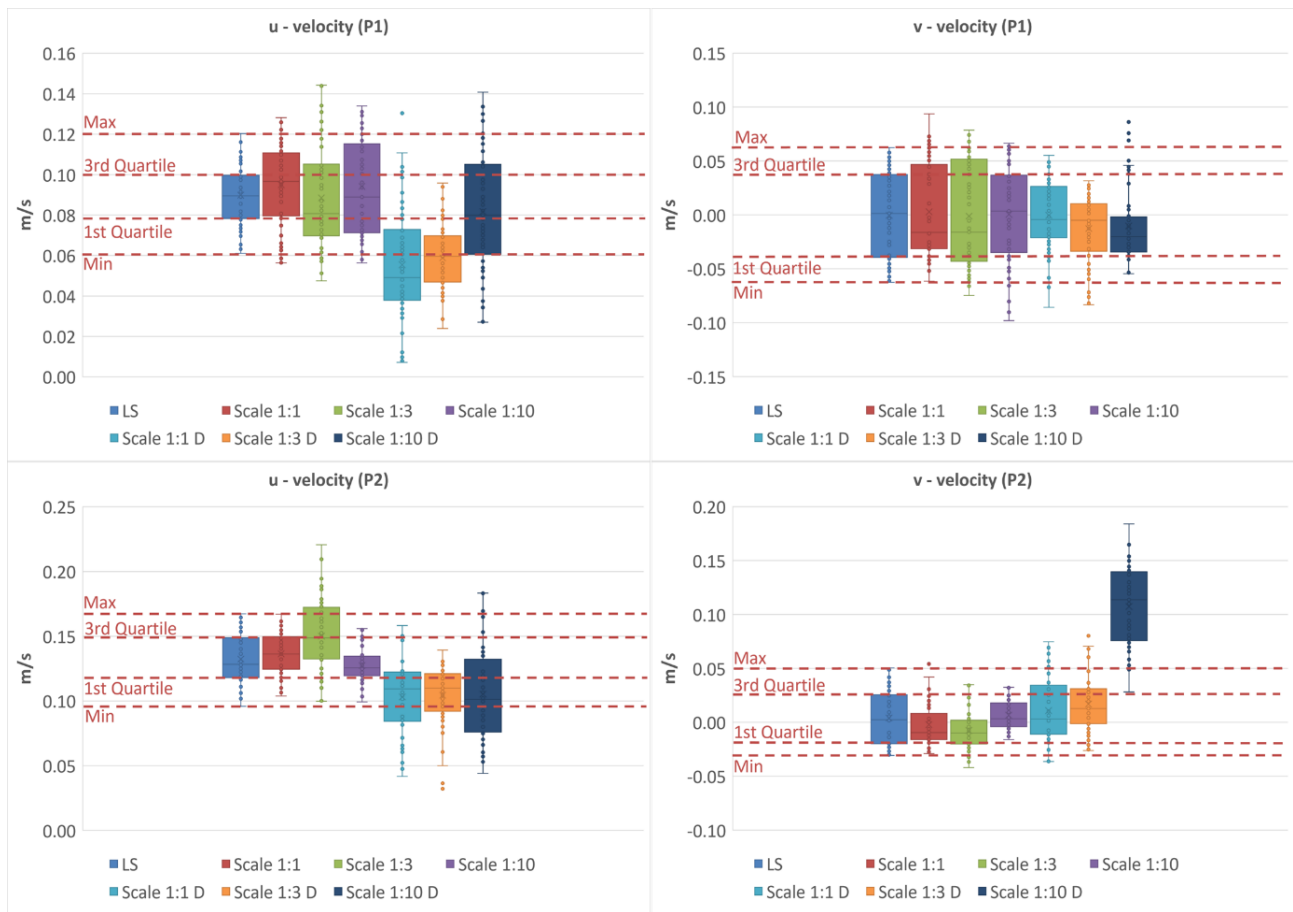


Fig. 7 Box-plot for P1 and P2 (D denotes the distorted model)

instance, the PPMC values for the scale of 1:1 at P1 and P2 are comparatively better than those of the scales of 1:3 and 1:10. The results of the undistorted models somehow show that the larger the scale, the worse the RMSE and PPMC values, except for the v-velocity at P2. For the distorted model, however, it becomes more complicated. As the scale becomes larger, neither of the distorted models shows consistent trends of RMSE and PPMC values for both velocities.

We present the box-plot for P1 and P2 in Fig. 7 to show the results for capturing 25–75% (first and third quartiles) as well as the minimum and maximum values of the observed data. One can see that 25–75% of the model results (v-velocity at P1 and u-velocity at P2) with a scale of 1:1 are in line with the LS experiment data; indeed, discrepancies are shown for u-velocity at P1 and v-velocity at P2 but significantly lower than those of the other scales. Another finding is that the discrepancies for 25–75% of the results become higher as the scale ratio increases, even worsening for the distorted models. All these findings point out that the scale effects exist for recirculating shallow flow and become progressively significant (to affect the flow characteristics) as the scale increases. In summary, the scale effects exist for both undistorted and distorted models that can be observed from the increase/decrease of the 25–75% or the minimum-maximum values of the results as the scale becomes larger.

3.3 Scale Effects for Non-Recirculating Flow Zone

In this section, the velocity results are presented at P3 and P4, see Fig. 8, in order to investigate whether the scale effects are significant for non-recirculating flow. As expected, no recirculation exists at P3 and P4, indicated by the velocity fluctuations with very low magnitude. For instance, the u-velocity at P3 has a value of approximately 0.115 m/s, thus being relatively constant over time. Similar insignificant fluctuations can also be observed at P4. Such fluctuations may be due to the difference in the turbulent scales since the Reynolds numbers vary between each case.

This phenomenon can also be explained by Fig. 9, showing the box-plot for P3 and P4, for which the results of the 1:1 scale are used as the basis. One can see that 25–75% of the results with the other scales (distorted and undistorted models) agree with the ones of the 1:1 scale. This finding clearly demonstrates that the scale effects do not apply to non-recirculating flow, where the vortices are absent.

3.4 Investigation of Energy Loss

We provide in this section the results for the pressure, velocity, and total heads to observe the role of the scale effects in contributing to energy loss. For this, the head measurement along the center of the section in the x-axis is shown in Fig. 10. The difference in energy loss is also summarized in Table 3, for which the results of the 1:1

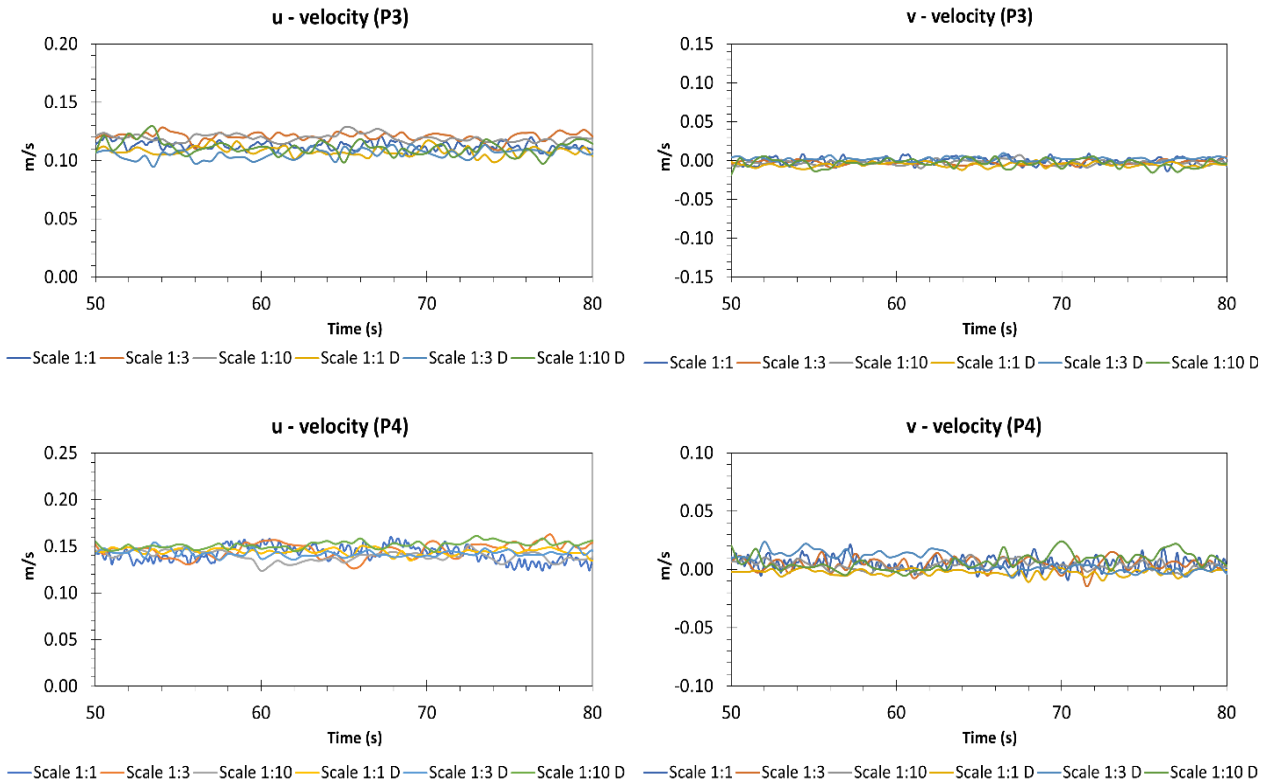


Fig. 8 Velocity profile – all cases at P3 and P4 (D denotes the distorted model)

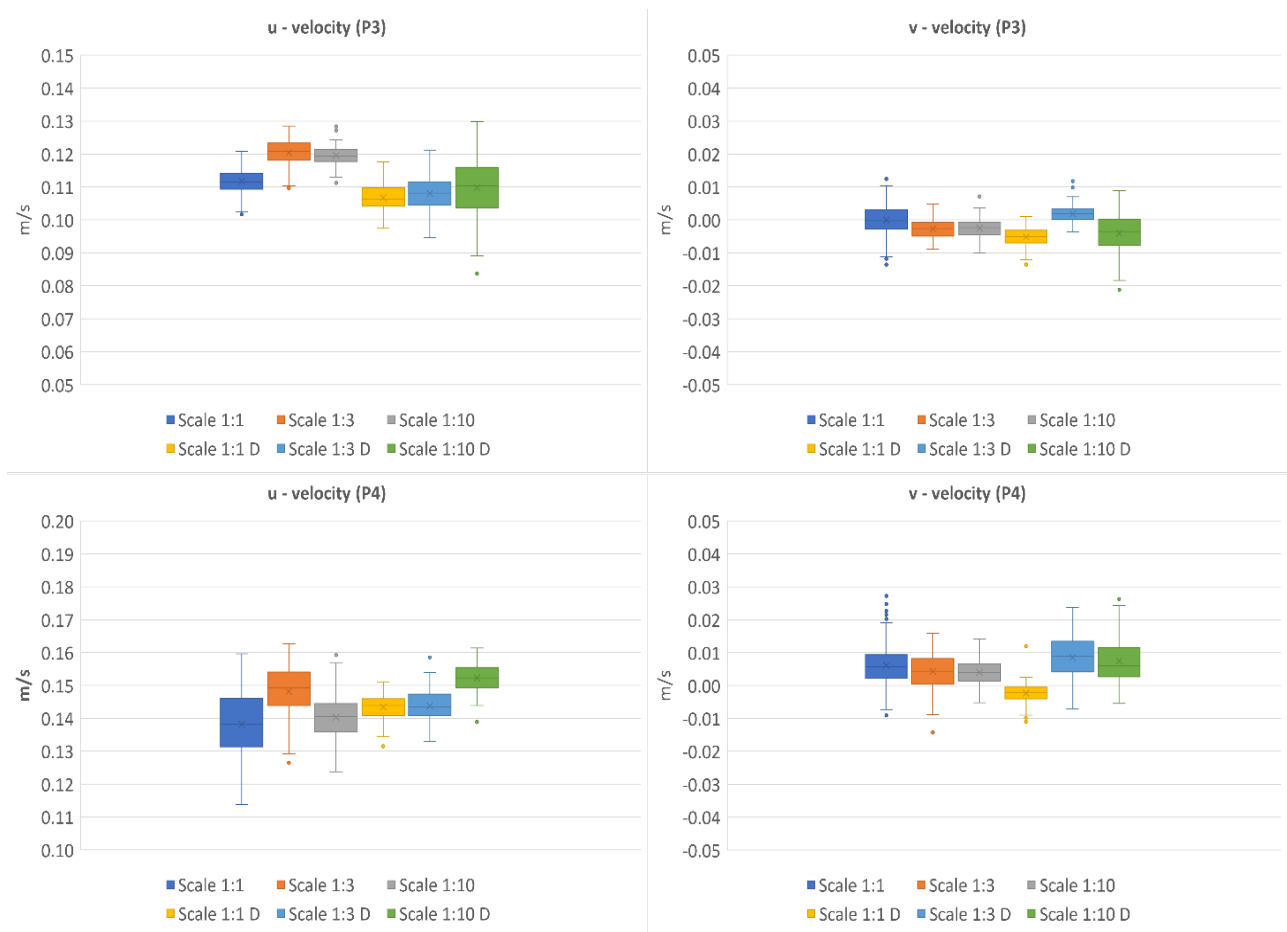


Fig. 9 Box-plot for P3 and P4 (D denotes the distorted model)

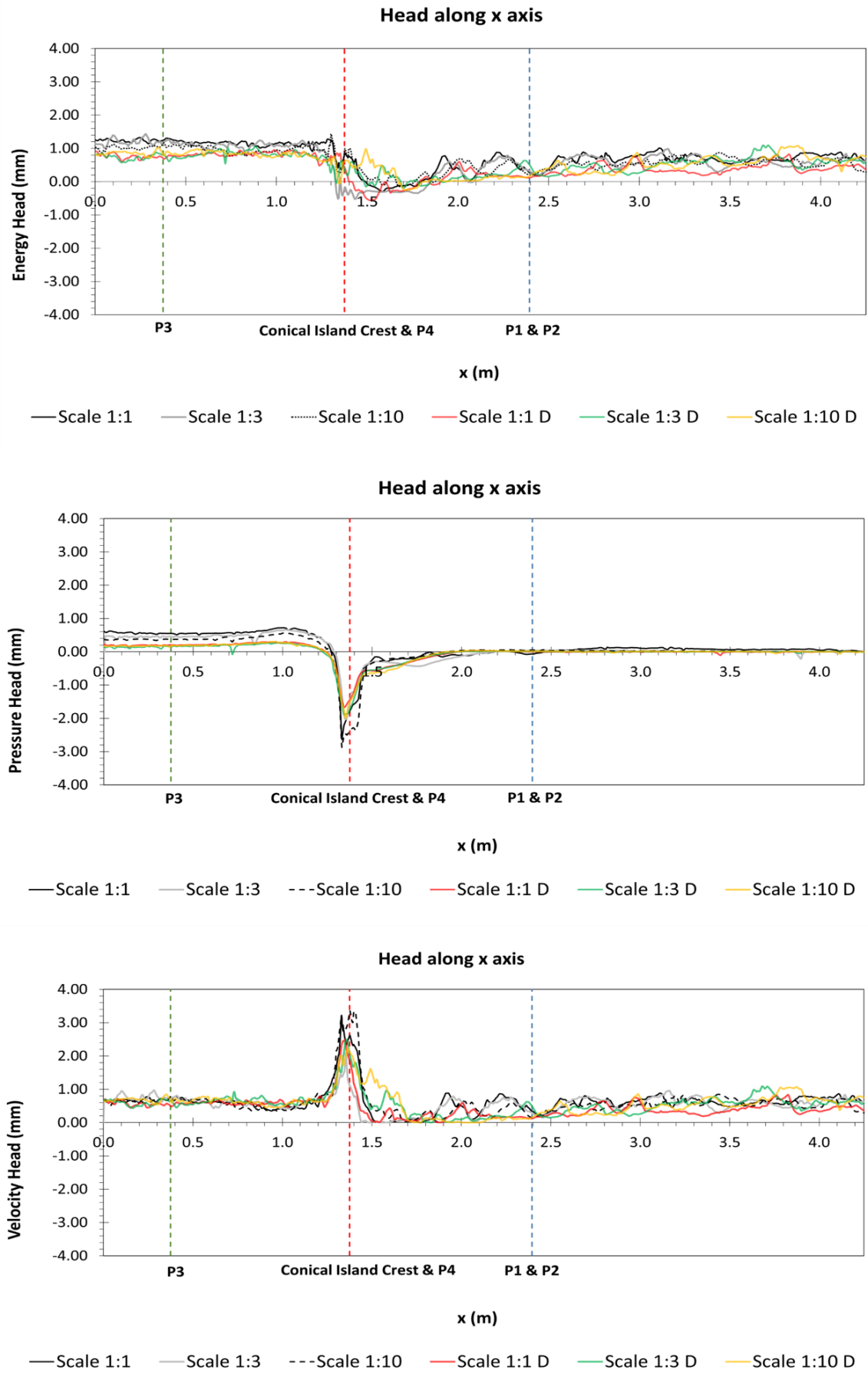


Fig. 10 Head along x-axis: total head (top), pressure head (middle), and velocity head (bottom) (D denotes the distorted model)

Table 3 Comparison of the energy loss after the conical island (D denotes the distorted model)

Energy Head Loss		
Scale 1	0.6020	mm
Scale 3	0.8106	mm
Scale 10	0.8440	mm
Scale 1 D	0.5554	mm
Scale 3 D	0.5084	mm
Scale 10 D	0.460549	mm
Delta Energy Head Loss to Scale 1		
Scale 3	34.65	%
Scale 10	40.20	%
Scale 1 D	7.74	%
Scale 3 D	15.54	%
Scale 10 D	23.49	%

scale are used as the basis. The equation used to calculate the energy loss (Δ_h) is expressed as follows:

$$\Delta_h = \frac{v_1^2 - v_2^2}{2 \times g} + \frac{(p_1 - p_2)}{g} \quad (17)$$

where v is the velocity, p is the pressure, and g is the gravitational acceleration. The velocity magnitudes and pressure values were obtained from the specific field using ParaView tool. Note that the pressure in OpenFOAM is density-normalized.

It can be seen from Fig. 10 that the scale effects cause differences in energy loss, which tend to increase as the scale increases. For example, significant differences in a velocity head are noticeable very close to (both in front of and behind) the conical island. Nevertheless, only negligible differences are observed for the pressure head in front of and behind the conical island. This can be interpreted as a condition with a relatively-constant depth but significantly different velocity due to the presence of recirculating flow.

Our results prove that the scale effects also contribute to the energy loss, which may occur due to differences in the vortex structures. Furthermore, as shown in Table 3, the distorted models tend to undermine the scale effects, which is probably caused by the lack of the von Kármán vortex, thus decreasing the overall energy loss.

3.5 Visualization for Velocity Magnitude and Vortex

We also provide visualizations of the detailed wakes to illustrate the implication of the scale effects, especially for the area behind the conical island. Note that the horizontal dimension and velocity values (for both

undistorted and distorted models) were adjusted with their respective scales back to a factor of 1:1 for direct comparison, but the vertical dimension for each model was kept to its original scale. All visualizations were made after shifting the time to ensure alignment with the same wake phase.

The streamline visualizations in Fig. 11 show that the von Kármán vortex street behind the conical island is quite different between the scale values of 1:1, 1:3 (undistorted), and 1:3 (distorted). For instance, the vortex for the 1:3 (undistorted) scale is less prominent than that of the 1:1 scale, becoming more inconspicuous using the 1:3 distorted model. In contrast, there is no vortex in front of the conical island, as expected, where the streamline pattern is relatively straight.

In Fig. 12, the visualization for the velocity magnitude is presented. For the 1:1 scale, it is clearly observed that the flow separation exists behind the conical island, where the recirculating flow dominantly appears, indicated by the wakes. The maximum velocity magnitude occurs at the top of the conical island due to the very shallow depth. The flow separation is still observable for the 1:3 scale (undistorted), albeit not as strong as the 1:1 scale. Further, the 1:3 scale (distorted) captures very weak flow separation.

In Fig. 13, we visualize the velocity magnitude captured in the YZ plane, focusing on the region behind the conical island (in line with P1 and P2). For the 1:1 scale, the turbulent structures prominently appear characterized by distinct von Karman vortex streets. The recirculation zone exhibits complex flow patterns due to the vortices and eddies. The result for the 1:3 scale (undistorted) reveals that the turbulent structures produce flow patterns like those of the 1:1 scale. However, for the 1:3 scale (distorted), notable differences in the turbulent structures are observed. The von Karman vortex street appears to be significantly diffused or decayed, suggesting that the variations in the Reynolds number may be responsible for altering the turbulent patterns.

Finally, we present in Fig. 14 the visualization for the velocity magnitude in the vertical direction. A strong vertical mixing appears behind the conical island for the 1:1 scale, which shows the 3D flow properties existing at this location, thus obviously being a non-hydrostatic phenomenon. For the 1:3 scale (undistorted), the vertical mixing behind the conical island is still observable and shows a similar pattern to that of the 1:1 scale. However, for the 1:3 scale (distorted), only a very weak vertical

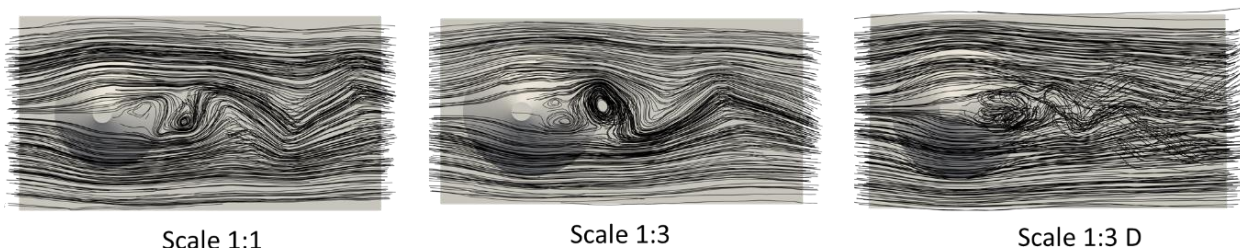


Fig. 11 Streamline visualization (D denotes the distorted model)

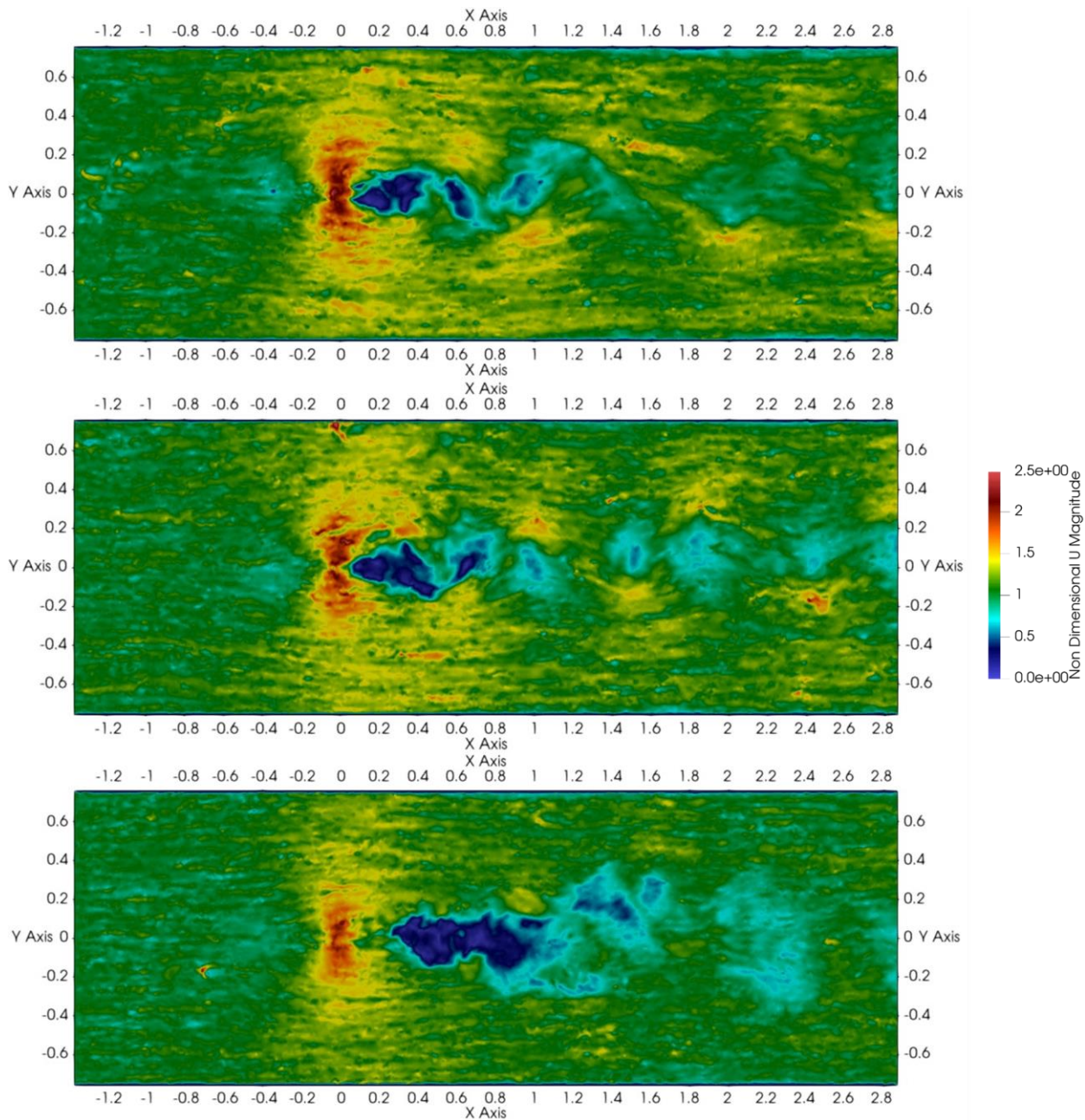


Fig. 12 Horizontal velocity magnitude distribution – scale 1:1 (top), 1:3 (middle), and 1:3 D (bottom)

mixing is observed behind the conical island, in which the velocity magnitudes show different patterns. In Fig. 13, one can also observe that the vertical characteristics of the velocity magnitude for the 1:3 scale (undistorted) are quite similar with those of the 1:1 scale. Nevertheless, the characteristics shown by the 1:3 (distorted) are highly different. Note that all the velocity values in Fig.12, Fig. 13, and Fig. 14 are of a non-dimensional form with respect to the free-stream velocity value.

4. CONCLUSION

The scale effects in the physical modeling of recirculating shallow flow have been investigated using the LES technique with a dynamic one-equation SGS model. In summary, the model was able to properly simulate the LS experiment data. Also, for the cases with the Froude similarity and $\lambda \neq 1$, the results showed that the scale effects were present in the form of differences in

vortices' period and magnitude. Especially for the recirculation zone, the undistorted models captured a weaker magnitude of vortices, becoming weaker with the distorted models. This clearly indicates that the scale effects predominantly appeared in the recirculation zones. The percentage error for the minimum value of u-velocity at P2 was 10.09% for the 1:3 scale (undistorted) but became 82.21% for the distorted model with the same scale. Additionally, the distorted model also induced notable discrepancies in characterizing the turbulent structures. The von Karman vortex street appeared to be significantly diffused or decayed, suggesting that the variations in the Reynolds numbers may be responsible for the alteration of turbulent patterns.

In contrast, for non-recirculating flow, i.e., in front of the conical island, only insignificant fluctuations were detected by the LES model either with the 1:1 scale, the undistorted, or distorted models. This shows that the scale

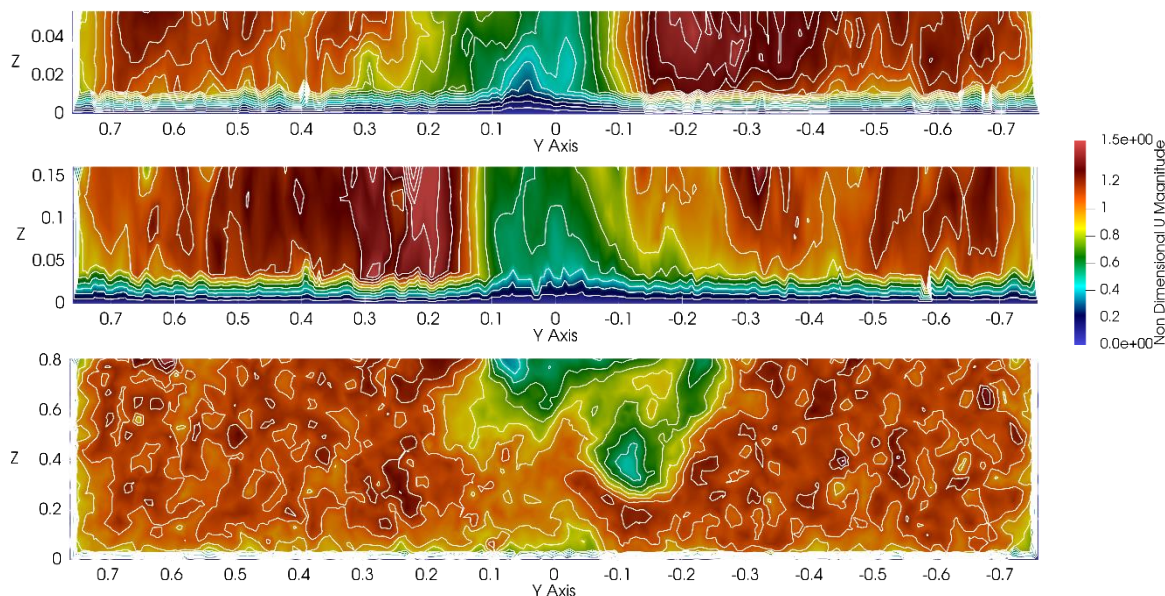


Fig. 13 Vertical velocity magnitude distribution in the YZ plane on P1 and P3 – scale 1:1 (top), 1:3 (middle), and 1:3 D (bottom)

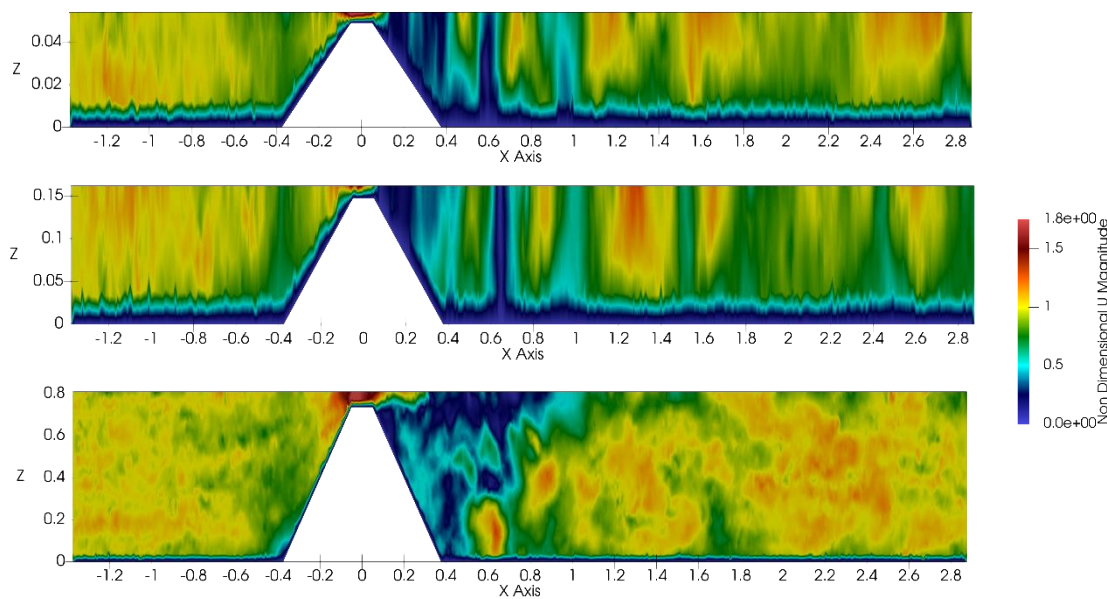


Fig. 14 Vertical velocity magnitude distribution in the XZ plane – scale 1:1 (top), 1:3 (middle), and 1:3 D (bottom)

effects do not apply to the non-recirculating zone, of which the streamline pattern is relatively straight without vortices. This evidence supports our hypothesis that the scale effects due to the Froude similarity are quite significant provided that recirculating turbulent flow occurs.

Future research could investigate the scale effects with the Reynolds similarity. Furthermore, mesh size influence is also worth mentioning for the scale effects' investigation. Additionally, future studies may explore other ways of modeling, such as employing a two-phase flow to account for the water depth effect or even various

types of the LES models that incorporate the other SGS models, such as the Wall Adapting Local Eddy-viscosity (WALE) model or SGS-free models. Also, the use of the DNS technique, which is regarded as the most 'physically-realistic' model is worth being investigated as it simply depends on the numerical approach to solve the Navier-Stokes equations, and does not require a turbulence model.

ACKNOWLEDGEMENTS

The authors are grateful to the Institute for Research and Community Service (Lembaga Penelitian dan

Pengabdian kepada Masyarakat) of Parahyangan Catholic University for supporting this work with a funding number III/LPPM/2023-02/35-P. Also, the computing resources of the UNPAR and the BINTEK laboratories are appreciated.

CONFLICT OF INTEREST

The authors declare no conflict of interest.

AUTHORS CONTRIBUTION

R. A. Tartandyo (data curation, formal analysis, investigation, software, visualization, writing – original draft); **B. M. Ginting** (conceptualization, formal analysis, funding acquisition, methodology, resources, supervision, writing – review & editing); **J. Zulfan** (formal analysis, project administration, resources).

REFERENCES

- Chanson, H. (2008). *Physical modelling, scale effects, and self-similarity of stepped spillway flows*. Proceedings of the World Environmental and Water Resources Congress 2008. [https://doi.org/10.1061/40976\(316\)624](https://doi.org/10.1061/40976(316)624)
- Chanson, H. (2009). Turbulent air–water flows in hydraulic structures: dynamic similarity and scale effects. *Environmental Fluid Mechanics*, 9(2), 125–142. <https://doi.org/10.1007/s10652-008-9078-3>
- Chanson, H., & Murzyn, F. (2008). *Froude similitude and scale effects affecting air entrainment in hydraulic jumps*. Proceedings of the World Environmental and Water Resources Congress 2008. [https://doi.org/10.1061/40976\(316\)240](https://doi.org/10.1061/40976(316)240)
- Chanson, H., Aoki, S., & Hoque, A. (2004). Physical modelling and similitude of air bubble entrainment at vertical circular plunging jets. *Chemical Engineering Science*, 59(4), 747–758. <https://doi.org/10.1016/j.ces.2003.11.016>
- Chaudhry, M. H. (1993). *Open-channel flow*. Prentice-Hall, Inc., Englewood Cliffs.
- Ferziger, J. H., & Perić, M. (1996) *Computational Methods for Fluid Dynamics*. Springer, Berlin. <https://doi.org/10.1007/978-3-642-97651-3>
- Fröhlich, J., & Rodi, W. (2002). Introduction to Large Eddy Simulation of Turbulent Flows. In B. Launder & N. Sandham (Eds.), *Closure Strategies for Turbulent and Transitional Flows* (pp. 267-298). Cambridge: Cambridge University Press. <https://doi.org/10.1017/CBO9780511755385.010>
- Ginting, B. M., & Ginting, H. (2019). Hybrid Artificial Viscosity–Central-Upwind Scheme for Recirculating Turbulent Shallow Water Flows. *Journal of Hydraulic Engineering*, 145(12), 04019041. [https://doi.org/10.1061/\(ASCE\)HY.1943-7900.0001639](https://doi.org/10.1061/(ASCE)HY.1943-7900.0001639)
- Heller, V. (2007). Massstabeffekte im hydraulischen Modell (Scale effects in hydraulic modelling). *Wasser Energie Luft*, 99(2), 153–159 [in German].
- Heller, V. (2011). Scale effects in physical hydraulic engineering models. *Journal of Hydraulic Research*, 49(3), 293–306. <https://doi.org/10.1080/00221686.2011.578914>
- Hughes, S. A. (1993). *Physical models and laboratory techniques in coastal engineering*. World Scientific, London.
- Kim, W. W., & Menon, S. (1995). *A new dynamic one-equation subgrid-scale model for large eddy simulations*. 33rd Aerospace Sciences Meeting and Exhibit, Reno, NV, United States. <https://doi.org/10.2514/6.1995-356>
- Lesieur, M., & Metais, O. (1996). New trends in large-eddy simulations of turbulence. *Annual Review of Fluid Mechanics*, 28(1), 45–82. <https://doi.org/10.1146/annurev.fl.28.010196.000401>
- Lloyd, P. M., & Stansby, P. K. (1997). Shallow-water flow around model conical islands of small side slope. II Submerged. *Journal of Hydraulic Engineering*, 123(12), 1068–1077. [https://doi.org/10.1061/\(ASCE\)0733-9429\(1997\)123:12\(1068\)](https://doi.org/10.1061/(ASCE)0733-9429(1997)123:12(1068))
- Martin, H., & Pohl, R. (2000). *Technische Hydromechanik 4 (Technical hydromechanics)*. Verlag für Bauwesen, Berlin [in German].
- Menon, S., & Yeung, P. K. (1994). *Analysis of subgrid models using direct and large-eddy simulations of isotropic turbulence*. Proc. AGARD 74th Fluid Dynamics Symp. on Application of Direct and Large Eddy Simulation to Transition and Turbulence, AGARD-CP-551.
- Menon, S., Yeung, P. K., & Kim, W. W. (1994). *Effect of subgrid models on the computed interscale energy transfer in isotropic turbulence*. 25th AIAA Fluid Dynamics Conference, Colorado Springs, CO, United States. <https://doi.org/10.2514/6.1994-2387>
- Novak, P., Guinot, V., Jeffrey, A., & Reeve, D. E. (2010). *Hydraulic modelling: an introduction: principles, methods and applications (1st ed.)*. CRC Press. <https://doi.org/10.1201/9781315272498>
- Novak, P., Moffat, A. I. B., Nalluri, C., & Narayanan, R. (2007). *Hydraulic Structures (4th ed.)*. CRC Press. <https://doi.org/10.1201/9781315274898>
- Ouro, P., Wilson, C. A. M. E., Evans, P., & Angeloudis, A. (2017). Large-eddy simulation of shallow turbulent wakes behind a conical island. *Physics of Fluids*, 29(12), 126601. <https://doi.org/10.1063/1.5004028>
- Piomelli, U. (1999). Large-eddy simulation: achievements and challenges. *Progress in Aerospace Sciences*, 35(4), 335–362. [https://doi.org/10.1016/S0376-0421\(98\)00014-1](https://doi.org/10.1016/S0376-0421(98)00014-1)
- Pope, S. (2000). *Turbulent Flows*. Cambridge: Cambridge University Press. <https://doi.org/10.1017/CBO9780511840531>

- Rodi, W. (2017). Turbulence modeling and simulation in hydraulics: A historical review. *Journal of Hydraulic Engineering*, 143(5), 03117001. [https://doi.org/10.1061/\(ASCE\)HY.1943-7900.0001288](https://doi.org/10.1061/(ASCE)HY.1943-7900.0001288)
- Sagaut, P. (2006). *Large eddy simulation for incompressible flows: an introduction (Third Ed.)*. Springer-Verlag Berlin Heidelberg.
- Sharma, H., Singh, D., & Singh, A. K. (2021). Large eddy simulation of film cooling over a flat plate in supersonic flow. *Journal of Thermal Science and Engineering Applications*, 13(4), 041019. <https://doi.org/10.1115/1.4049342>
- Singh, D., Udayraj Singh, A. N., & Handique, J. (2022). Experimental and LES study of unconfined jet impingement on a smooth flat heated plate with slots of different widths. *Experimental Heat Transfer* <https://doi.org/10.1080/08916152.2022.2096153>
- Stoesser, T. (2014). Large-eddy simulation in hydraulics: Quo Vadis? *Journal of Hydraulic Research*, 52(4), 441–452. <https://doi.org/10.1080/00221686.2014.944227>
- Suerich-Gulick, F., Gaskin, S. J., Villeneuve, M., & Parkinson, É. (2014). Free surface intake vortices: scale effects due to surface tension and viscosity. *Journal of Hydraulic Research*, 52(4), 513–522. <https://doi.org/10.1080/00221686.2014.905503>
- Torres, C., Borman, D., Matos, J., & Neeve, D. (2022). CFD modeling of scale effects on free-surface flow over a labyrinth weir and spillway. *Journal of Hydraulic Engineering*, 148(7), 4022011. [https://doi.org/10.1061/\(ASCE\)HY.1943-7900.0001989](https://doi.org/10.1061/(ASCE)HY.1943-7900.0001989)
- Tullis, B. (2018). *Size-Scale Effects of Labyrinth Weir Hydraulics*. 7th IAHR International Symposium on Hydraulic Structures, Aachen, Germany. <https://doi.org/10.15142/T3R06F>
- Versteeg, H. K., & Malalasekera, W. (2007). *An introduction to computational fluid dynamics: the finite volume method 2nd edition*. Edinburgh: Pearson Prentice Hall
- Yoshizawa, A. (1993). Bridging between eddy-viscosity-type and second-order turbulence models through a two-scale turbulence theory. *Physical Review E*, 48(1), 273–281. <https://doi.org/10.1103/PhysRevE.48.273>